Measuring optical turbulence with FEELINGS optical ground station

Florian Quatresooz[a], Cyril Petit[a], Kyliann Robert[a], and Nicolas Védrenne[a]

[a]DOTA, ONERA, Université Paris-Saclay, 92320 Châtillon, France

ABSTRACT

Monitoring atmospheric turbulence is key for improving the reliability of future free-space optical communication networks and developing efficient mitigation techniques. Of particular interest is the knowledge of the refractive index structure parameter (C_n^2) profile along the line of sight, that can be obtained thanks to the Single Coupled Slopes and Intensities Detection and Ranging (SCO-SLIDAR) method. This method is based on the exploitation of spatial covariances of wavefront slopes and intensities gathered by a Shack-Hartmann wavefront sensor (SHWFS). Furthermore, the joint exploitation of temporal covariances of SHWFS measurements offers the perspective of a simultaneous wind profile measurement. We present in this paper our extensions to the SCO-SLIDAR method to extract the wind profile from SHWFS data. Our approach is first validated on experimental data collected with the PICOLO turbulence emulation bench before being applied to SHWFS measurements obtained during a GEO to ground optical link with FEELINGS optical ground station.

Keywords: Free-space optical communications, optical turbulence, wind profiling

1. INTRODUCTION

As the technology for free-space optical communications (FSOC) between the ground and satellites is maturing, much efforts are still required to ensure the reliable operation of future FSOC networks. A major challenge is atmospheric turbulence, impacting the propagation of optical waves through the atmosphere and degrading communication signals.[1,2] To accurately characterize and potentially mitigate this effect (e.g., using adaptive optics), the knowledge of both the refractive index structure parameter (C_n^2) profile and wind profile is paramount.[3] This knowledge is especially important along the line of sight of optical links in order to estimate and predict optical communication performance.[4,5]

Monitoring of C_n^2 profiles is usually achieved remotely (i.e., without requiring in-situ measurements) with dedicated optical turbulence (OT) monitoring instruments such as SCIntillation Detection And Ranging (SCIDAR) or Slope Detection and Ranging (SLODAR) instruments.[6,7] However, these instruments, relatively large and costly, were developed for astronomical applications and require binary stars for operation. Other compact instruments using a single source exist, such as the Differential Image Motion Monitor (DIMM) instrument measuring the seeing (i.e., an integrated parameter of the C_n^2 profile) or the Multi-Aperture Scintillation Sensor (MASS) instrument that gives access to a few layer C_n^2 profile.[8,9] For optical communication applications, new generation OT monitoring instruments are being developed, including the Shack-Hartmann Image Motion Monitor (SHIMM) instrument.[10,11] However, these different instruments are unlikely to deliver C_n^2 profiles aligned with the optical link line of sight. As an alternative, the Single Coupled Slopes and Intensities Detection and Ranging (SCO-SLIDAR) method enables to estimate C_n^2 profiles along the line of sight from Shack-Hartmann wavefront sensor (SHWFS) measurements of a single source (e.g., natural star, laser guide star, or satellite laser terminal).[12]

Regarding the estimation of wind profiles, it can be conducted with SCIDAR instruments[13,14] or from SHWFS observations of multiple guide stars.[15,16] However, alternative approaches are necessary to estimate the wind profile from single sources.

In this work, we present our extensions to the SCO-SLIDAR method to measure both C_n^2 and wind profiles along the line of sight, based on the exploitation of spatio-temporal covariances from SHWFS measurements. Our approach is detailed in Section 2. Section 3 presents the experimental validation of the method with the PICOLO turbulence emulation bench,[17] while Section 4 shows our first results of C_n^2 and wind speed estimation from SHWFS data collected during a GEO to ground optical link with FEELINGS optical ground station (OGS).[18]

2. WIND PROFILE ESTIMATION FROM SCO-SLIDAR APPROACH

First, key equations of the SCO-SLIDAR are reminded in Section 2.1, before being extended to wind profile estimation in Section 2.2.

2.1 SCO-SLIDAR

The SCO-SLIDAR approach makes use of SHWFS data from a single source and is based on the computation of spatial covariances between subaperture pairs. Both measured intensities and slopes in the SH subapertures are exploited. The fluctuations of the intensity in a subaperture m is denoted δi_m (normalized), while the slopes are noted $s_{x,m}$ and $s_{y,m}$, for the x- and y-directions respectively.

The key equations of the SCO-SLIDAR approach[12,19] are

$$\langle \delta i_m \; \delta i_n \rangle = \int_0^{+\infty} C_n^2(z) \; w_i(z, \boldsymbol{d}_{mn}) \; \mathrm{d}z \tag{1}$$

$$\langle s_{x,m} \; s_{x,n} \rangle = \int_0^{+\infty} C_n^2(z) \; w_{s_x}(z, \boldsymbol{d}_{mn}) \; \mathrm{d}z \tag{2}$$

$$\langle s_{x,m} \; s_{y,n} \rangle = \int_0^{+\infty} C_n^2(z) \; w_{s_{xy}}(z, \boldsymbol{d}_{mn}) \; \mathrm{d}z \tag{3}$$

$$\langle s_{y,m} \; s_{y,n} \rangle = \int_0^{+\infty} C_n^2(z) \; w_{s_y}(z, \boldsymbol{d}_{mn}) \; \mathrm{d}z, \tag{4}$$

where $\boldsymbol{d}_{mn}$ is the subaperture pair (m,n) spacing distance and z is the distance along the propagation path. In (1) to (4), the first terms refer to the covariances of intensity (resp. slopes) between subapertures m and n, with $\langle \cdot \rangle$ depicting the expectation operator. These covariances are measured from temporal averaging over numerous frames (typically, 10000 collected at 1 to 2 kHz) of the SHWFS camera and are averaged for subaperture pairs having the same spacing, leading to so-called *covariance maps*.

Equations (1) to (4) involve the *weighting functions* of the instrument, i.e., $w_i(z, \boldsymbol{d}_{mn})$, $w_{s_x}(z, \boldsymbol{d}_{mn})$, $w_{s_{xy}}(z, \boldsymbol{d}_{mn})$ and $w_{s_y}(z, \boldsymbol{d}_{mn})$. Assuming plane waves, small perturbations and a modified von Kármán spectrum for describing the refractive index fluctuations, they are given by

$$w_i(z, \boldsymbol{d}_{mn}) \;=\; \mathscr{F}^{-1}\left\{4 \; \hat{P}^2(\boldsymbol{f}) \; \tilde{W}_\varphi(\boldsymbol{f}) \left(\sin(\pi \lambda z f^2)\right)^2\right\}(\boldsymbol{d}_{mn}) \tag{5}$$

$$w_{s_x}(z, \boldsymbol{d}_{mn}) \;=\; \mathscr{F}^{-1}\left\{\lambda^2 f_x^2 \; \hat{P}^2(\boldsymbol{f}) \; \tilde{W}_\varphi(\boldsymbol{f}) \left(\cos(\pi \lambda z f^2)\right)^2\right\}(\boldsymbol{d}_{mn}) \tag{6}$$

$$w_{s_{xy}}(z, \boldsymbol{d}_{mn}) \;=\; \mathscr{F}^{-1}\left\{\lambda^2 f_x f_y \; \hat{P}^2(\boldsymbol{f}) \; \tilde{W}_\varphi(\boldsymbol{f}) \left(\cos(\pi \lambda z f^2)\right)^2\right\}(\boldsymbol{d}_{mn}) \tag{7}$$

$$w_{s_y}(z, \boldsymbol{d}_{mn}) \;=\; \mathscr{F}^{-1}\left\{\lambda^2 f_y^2 \; \hat{P}^2(\boldsymbol{f}) \; \tilde{W}_\varphi(\boldsymbol{f}) \left(\cos(\pi \lambda z f^2)\right)^2\right\}(\boldsymbol{d}_{mn}), \tag{8}$$

where $\mathscr{F}^{-1}\{\cdot\}(\boldsymbol{d}_{mn})$ denotes the 2D inverse Fourier transform ($\boldsymbol{f} = (f_x, f_y)$ is the spatial frequency, with $f = |\boldsymbol{f}|$) sampled for $\boldsymbol{d}_{mn}$ positions, $\hat{P}(\boldsymbol{f})$ is the Fourier transform of the subaperture averaging function $P(\boldsymbol{x})$ corresponding to the subaperture shape (e.g., circular, square), and $\tilde{W}_\varphi(\boldsymbol{f})$ is the power spectrum of the phase without the $C_n^2(z)$ dependency, i.e., $W_\varphi(\boldsymbol{f}) = C_n^2(z)\tilde{W}_\varphi(\boldsymbol{f})$. In the case of a modified von Kármán spectrum,

$$\tilde{W}_\varphi(\boldsymbol{f}) = 0.033 \; \frac{(2\pi)^{4/3}}{\lambda^2} \; \left(f^2 + \frac{1}{L_0^2}\right)^{-11/6} \; \exp\left(-\left(\frac{2\pi l_0}{5.92} f\right)^2\right),$$

with l_0 the inner scale of turbulence and L_0 the outer scale of turbulence. The wavelength is depicted by λ.

The SCO-SLIDAR approach aims to recover the C_n^2 profile from the observed covariance maps, knowing the instrument weighting functions. An inversion problem is defined, that is solved with a Maximum A Posteriori (MAP) estimator.[20,21] Cross-covariances between intensity and slopes are not exploited in this paper.

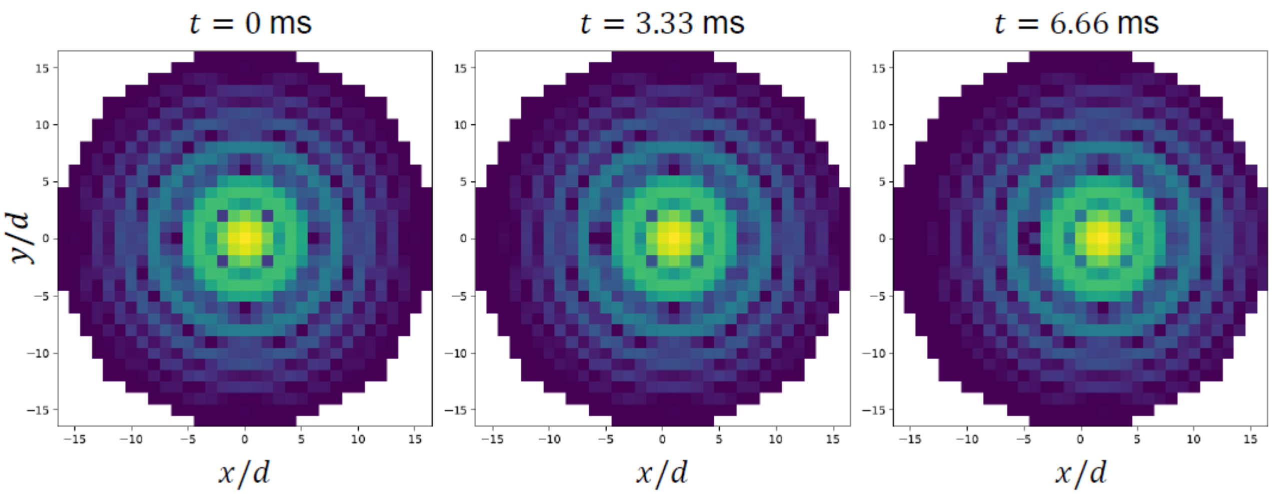

(a) Spatio-temporal covariance maps of intensity for a single turbulent layer at 10 km and moving at 10 m/s.

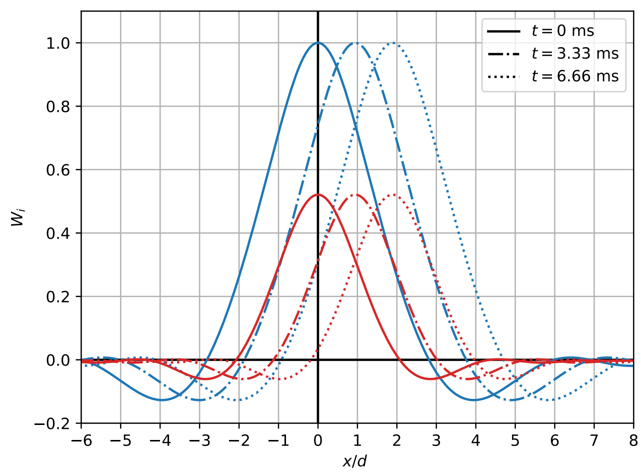

(b) 1D slice along x-axis of intensity covariance maps for two layers (5 km (red) and 10 km (blue), both moving at 10 m/s).

Figure 1: Example of theoretical spatio-temporal covariance maps of intensity (normalized).

2.2 Wind profile estimation

For estimating wind profile, spatio-temporal covariance maps are exploited, adding the temporal dimension. From SHWFS data, they are computed by delaying frames in the temporal average (i.e., over the numerous frames) used for estimating covariances.

Assuming Taylor frozen flow, the velocity of turbulent layers leads to translations of the spatial covariances maps, proportional to the layer wind speed and following its wind direction.[22,23] Hence, the theoretical weighting functions of the SCO-SLIDAR approach are adapted to include the temporal delay and the effect of wind velocity $\boldsymbol{v}(z)$ for the turbulent layers with the addition of a complex exponential $\exp\left(-\jmath 2\pi t \boldsymbol{v}(z) \cdot \boldsymbol{f}\right)$, as originally suggested for intensity fluctuations.[24] For example, the intensity weighting functions is given by

$$w_i(z, \boldsymbol{d}_{mn}, t) \; = \; \mathscr{F}^{-1}\left\{4\ \hat{P}^2(\boldsymbol{f})\ \tilde{W}_\varphi(\boldsymbol{f})\left(\sin(\pi\lambda z f^2)\right)^2\ \exp\left(-\jmath 2\pi t \boldsymbol{v}(z) \cdot \boldsymbol{f}\right)\right\}(\boldsymbol{d}_{mn}). \tag{9}$$

Equations (6) to (8) are adapted accordingly.

Table 1: Theoretical and estimated values for PICOLO parameters.

Layer	z [km]	C_n^2 dz [m$^{1/3}$]	Wind speed [m/s]	Estimated C_n^2 dz [m$^{1/3}$]	Estimated wind speed [m/s]
1 (L)	0	2.56×10^{-11}	5 (rot. right)	1.78×10^{-11}	5 (rot. right)
2 (M)	2.88	1.40×10^{-11}	10 (rot. right)	8.73×10^{-12}	10 - 12.5 (rot. right)
3 (H)	57.8	1.01×10^{-12}	20 (rot. left)	9.28×10^{-13}	20 - 25 (rot. left)

Figure 1a presents the theoretical spatio-temporal covariance maps of intensity for a single turbulent layer located at 10 km and moving at 10 m/s, for the specific SH configuration of FEELINGS ground station (17 × 17 SH, telescope diameter of 60 cm). The associated subaperture spacing d is 3.53 cm, and the operating wavelength is 1550 nm. The chosen temporal delays (3.33 ms and 6.66 ms) are such that the translation due to the wind speed in the successive figures is close to one subaperture spacing. This is further illustrated in Figure 1b, showing one-dimensional (1D) slices taken along the x-axis. The theoretical response for a layer at 5 km moving at the same speed (i.e., 10 m/s) is also depicted (red curve), highlighting that layers with the same displacements lead to the same motion in the covariance maps. Hence, their peaks will be superimposed and challenge layer identification, as discussed in Section 4.

The color scale is normalized by the magnitude of the covariance peak at 0 ms. In practice, the magnitude of this main peak is expected to decrease with the temporal delay, as the validity of the Taylor hypothesis is reduced.

3. EXPERIMENTAL VALIDATION WITH TURBULENCE EMULATION

Experimental validation of the SCO-SLIDAR and wind estimation approaches is conducted with PICOLO, that is a turbulence emulator bench equipped with adaptive optics (AO).[17] It represents a satellite LEO communication at 10° elevation (downlink) thanks to three rotating phase screens. The AO system contains a 8 × 8 SHWFS and the modelled telescope diameter is 40 cm (i.e., the subaperture spacing projected on the telescope aperture is $d = 5$ cm). The operating wavelength is 1550 nm. The rotation speeds of the phase screens can be chosen, while the equivalent C_n^2 dz's of each screen are fixed and given in the left part of Table 1. The screen altitudes are also fixed: one screen is in the pupil (L, low altitude), one is located at 2.88 km (M, mid altitude), and the last screen is at 57.8 km (H, high altitude).

For the configuration detailed in the left part of Table 1, C_n^2 dz is estimated with the SCO-SLIDAR approach. It shows a slight underestimation of C_n^2 dz at low and high altitudes, while this underestimation is more important for the mid altitude screen. Proper calibration of the SHWFS and the intensity and slope estimation algorithm is expected to reduce this underestimation.

Regarding the wind speeds of each layer, they are measured from the sequence of spatio-temporal covariance maps relying on a peak detection and tracking algorithm, as depicted in Figure 2. The velocity v of the layer is computed from the measured displacement in pixels n_{pixels} and with the relationship $v = n_{\text{pixels}} \frac{d}{t}$, for each direction. With PICOLO, only one direction can be used, associated to the phase screen rotation (rot.), either left or right.

Figure 2 leads to important comments:

- The intensity spatio-temporal covariance maps show two distinct turbulent layers, with one moving rapidly to the left (associated to the high altitude layer) and another one moving to the right (associated to the mid altitude layer). The layer in the pupil is not visible as it does not introduce intensity fluctuations.
- On the contrary, the covariance maps for the slopes in the x-direction enable to identify the two bottom layers. These layers first appear superimposed, before being clearly separated (e.g., at 20 ms).
- With our current peak detection and tracking approach, the estimation of the wind speed is limited by the spatial resolution of the covariance maps, i.e., the distance d, leading to the ranges of estimated speeds presented on the right part of Table 1.

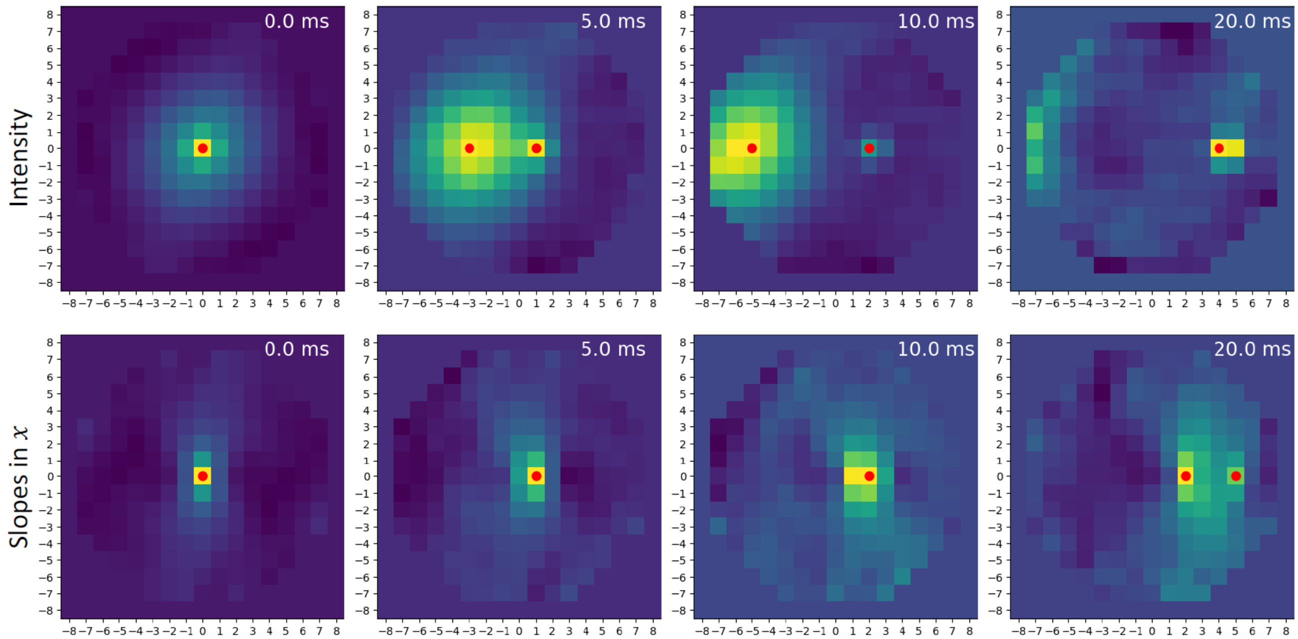

Figure 2: Sequence of measured spatio-temporal covariance maps with the PICOLO bench (normalized color scale).

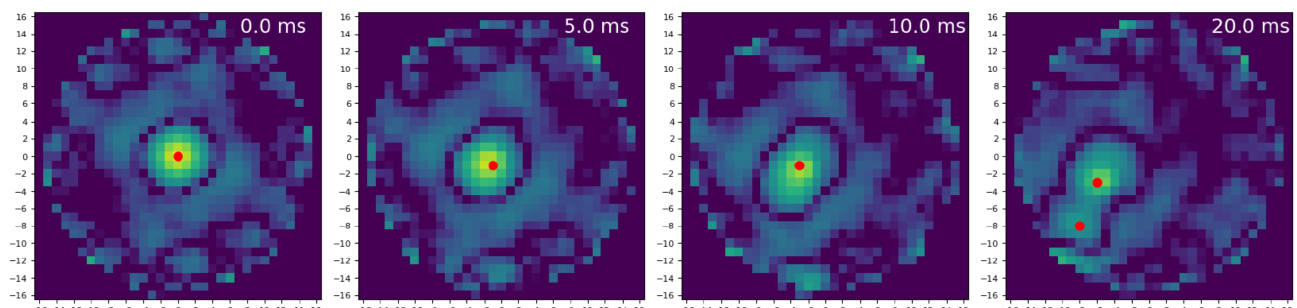

Figure 3: Sequence of measured intensity spatio-temporal covariance maps with FEELINGS on 23/09/2024 at 15h03 (normalized color scale for 0 ms, based on the logarithm in base 10 of the amplitude).

4. APPLICATION TO FEELINGS MEASUREMENTS

On-sky experiments have been conducted with FEELINGS optical ground station and TELEO payload (34° elevation link, with a GEO satellite, downlink), for several days in September 2024.[18] As preliminary results, measurements collected on September 23, 2024, at 15h03 (UTC time) are exploited to estimate the C_n^2 profile and wind speed. SHWFS data are collected in closed loop and are first converted to pseudo-open loop measurements, before computing the observed covariance maps.

The spatio-temporal covariance maps are shown in Figure 3, for the intensity only as the extraction of relevant features from slopes covariance maps is ongoing. They enable to identify two turbulent layers having for wind speed 11.8 m/s (10.6 m/s in x and 5.3 m/s in y), and 19.9 m/s (14.1 m/s in x and 14.1 m/s in y), highlighting the exploitability of FEELINGS' SHWFS data for wind speed estimation. They also show the limitation of the Taylor hypothesis, with temporal decorrelation appearing progressively (magnitude of the peak is decreasing, as seen with the color varying from yellow to green and then blue).

Comparisons of the measured wind speed with meteorological data from ECMWF ERA5 database[25] and Weather Research and Forecasting (WRF) simulations[26] are shown in Figure 4. The estimated C_n^2 profile from the SCO-SLIDAR method is also depicted. A possible identification of the two turbulent layers for which wind

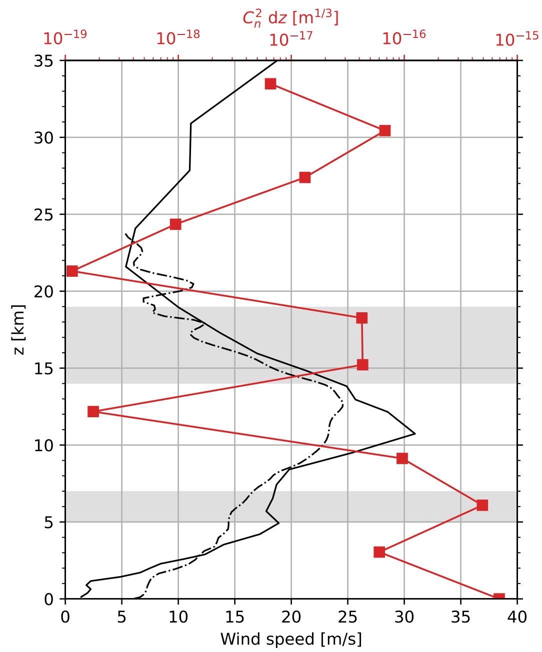

Figure 4: Wind profile from ERA5 data (plain line) and WRF simulations (dash-dotted line) and reconstructed C_n^2 profile from SCO-SLIDAR approach.

speeds have been estimated is depicted by the gray areas. The wind speed estimates appear to be realistic and in agreement with meteorological data, even though layer identification remain challenging and is part of future work, with layer altitudes that can potentially be estimated from the widths of the peaks in the spatio-temporal covariance maps.[22]

The strong turbulent layer located at high altitude ($\sim$ 30 km) in Figure 4 is probably not realistic and associated to biases in the SCO-SLIDAR model, most likely arising from phenomena not modelled in the theoretical weighting functions (e.g., vibrations, tracking error and mis-pointing that could lead to intensity variations). The wind speed of the turbulent layer close to ground cannot be sensed with the intensity spatio-temporal covariance maps and require the exploitation of slopes spatio-temporal covariance maps.

5. CONCLUSION

This work provides extensions to the SCO-SLIDAR approach to estimate the velocity of turbulent layers based on spatio-temporal covariance maps of intensities and slopes measured with a SHWFS. The approach is validated with the PICOLO turbulence emulator bench, highlighting the need for both intensity and slope measurements, and first on-sky results with FEELINGS OGS are shown.

From spatio-temporal covariance maps, the wind speed is estimated using a peak detection and tracking algorithm. This approach is limited by the pixel resolution of the SH geometry and associated to challenges for turbulent layer identification.

Future work includes the estimation of continuous wind profile (including wind direction), the study of temporal decorrelation, and the validation of C_n^2 and wind profiles measured at FEELINGS OGS. A joint approach for estimating both C_n^2 and the wind speed is under study.

ACKNOWLEDGMENTS

The authors acknowledge Airbus Defence and Space for the fruitful discussions and their help during the TELEO campaigns, within the framework of the MADIRAN project (DGA n°2023 99 0906) and the support from CNES.

F. Quatresooz's work is conducted within the framework of a joint ONERA/ESA postdoctoral research program, through the ESA Open Space Innovation Platform (contract number 4000146151).

REFERENCES

[1] Andrews, L. C. and Phillips, R. L., "Laser beam propagation through random media," *Laser Beam Propagation Through Random Media: Second Edition* (2005).

[2] Quatresooz, F. and Oestges, C., "Cn2 Modelling for Free-Space Optical Communications: a Review," *IEEE Access* (2025).

[3] Robles, P., Petit, C., Conan, J.-M., Benammar, B., and Neichel, B., "Predictive adaptive optics for satellite tracking applications: optical communications and satellite observation," in [*Adaptive Optics Systems VIII*], **12185**, 917–931, SPIE (2022).

[4] Paillier, L., Lai-Tim, Y., Poiron, A., Klotz, E., Lefebvre, S., Musso, C., Fusco, T., Petit, C., Bonnefois, A. M., Chalali, E., Caillault, K., Hespel, L., Krafft, L., Montri, J., Quatresooz, F., Poulenard, S., and Védrenne, N., "Propagation channel assessment for GEO feeder links," in [*2023 IEEE International Conference on Space Optical Systems and Applications (ICSOS)*], 93–102, IEEE (2023).

[5] Vedrenne, N., Bonnefois, A., Petit, C., Chalali, E., Lai-Tim, Y., Krafft, L., François, G., Caillault, K., Bedoya-Velásquez, A. E., Barbon-Dubosc, D., et al., "First results of ground to GEO optical links channel monitoring with FEELINGS," in [*International Conference on Space Optics (ICSO 2024)*], (2024).

[6] Wilson, R. W., "SLODAR: measuring optical turbulence altitude with a Shack–Hartmann wavefront sensor," *Monthly Notices of the Royal Astronomical Society* **337**(1), 103–108 (2002).

[7] Osborn, J., Wilson, R., Sarazin, M., Butterley, T., Chacón, A., Derie, F., Farley, O., Haubois, X., Laidlaw, D., LeLouarn, M., et al., "Optical turbulence profiling with Stereo-SCIDAR for VLT and ELT," *Monthly Notices of the Royal Astronomical Society* **478**(1), 825–834 (2018).

[8] Tokovinin, A., "From differential image motion to seeing," *Publications of the Astronomical Society of the Pacific* **114**(800), 1156 (2002).

[9] Kornilov, V., Tokovinin, A. A., Vozyakova, O., Zaitsev, A., Shatsky, N., Potanin, S. F., and Sarazin, M. S., "MASS: a monitor of the vertical turbulence distribution," in [*Adaptive Optical System Technologies II*], **4839**, 837–845, SPIE (2003).

[10] Griffiths, R., Osborn, J., Farley, O., Butterley, T., Townson, M. J., and Wilson, R., "Demonstrating 24-hour continuous vertical monitoring of atmospheric optical turbulence," *Opt. Express* **31**, 6730–6740 (2 2023).

[11] Beesley, L. F., Griffiths, R., Hartley, K., Farley, O. J. D., Quatresooz, F., Rodríguez-Gómez, A., Comerón, A., Townson, M., Alaluf, D., and Osborn, J., "Demonstration of 24-hour continuous optical turbulence monitoring in a city," *Opt. Express* **33**(5), 10140–10149 (2025).

[12] Védrenne, N., Michau, V., Robert, C., and Conan, J.-M., "Cn2 profile measurement from Shack-Hartmann data," *Optics letters* **32**(18), 2659–2661 (2007).

[13] Prieur, J.-L., Avila, R., Daigne, G., and Vernin, J., "Automatic determination of wind profiles with generalized SCIDAR," *Publications of the Astronomical Society of the Pacific* **116**(822), 778 (2004).

[14] Osborn, J., Butterley, T., Townson, M., Reeves, A., Morris, T., and Wilson, R., "Turbulence velocity profiling for high sensitivity and vertical-resolution atmospheric characterisation with stereo-scidar," *Monthly Notices of the Royal Astronomical Society* , stw2685 (2016).

[15] Guesalaga, A., Neichel, B., Cortés, A., Béchet, C., and Guzmán, D., "Using the and wind profiler method with wide-field laser-guide-stars adaptive optics to quantify the frozen-flow decay," *Monthly Notices of the Royal Astronomical Society* **440**(3), 1925–1933 (2014).

[16] Cortés, A., Neichel, B., Guesalaga, A., Osborn, J., Rigaut, F., and Guzman, D., "Atmospheric turbulence profiling using multiple laser star wavefront sensors," *Monthly Notices of the Royal Astronomical Society* **427**(3), 2089–2099 (2012).

[17] Robles, P., Petit, C., Velluet, M.-T., Le Leuch, L., Montmerle-Bonnefois, A., Paillier, L., Conan, J.-M., Cassaing, F., Montri, J., Neichel, B., et al., "Emulating and characterizing strong turbulence conditions for space-to-ground optical links: the PICOLO bench," *Journal of Astronomical Telescopes, Instruments, and Systems* **9**(4), 049002–049002 (2023).

[18] J.C. Richard, S. Poulenard , X. Gnata , L. Coret , T. Anfray , M. Crosnier , T. Marduel , L. Zurawski , S. Montigaud , F. Lacoste, J. Sommer, G. Artaud, B. Benammar , E. Samain , T. Lanz , E. Bondoux , A. Bonnefois , C. Petit, N. Védrenne , A. Schimpf, H. Forriere , "In orbit testing of GEO feeder links with TELEO," in [*International Conference on Space Optics (ICSO 2024)*], (2024).

[19] Robert, C., Conan, J.-M., Michau, V., Fusco, T., and Vedrenne, N., "Scintillation and phase anisoplanatism in Shack-Hartmann wavefront sensing," *JOSA A* **23**(3), 613–624 (2006).

[20] Védrenne, N., *Propagation optique et correction en forte turbulence*, PhD thesis (2008).

[21] Voyez, J., Robert, C., Michau, V., Conan, J.-M., and Fusco, T., "Accurate measurement of Cn2 profile with Shack-Hartmann data," in [*Adaptive Optics Systems III*], **8447**, 1718–1727, SPIE (2012).

[22] Ogane, H., Ono, Y., Minowa, Y., Oya, S., Terao, K., Akasawa, T., Homan, R., and Akiyama, M., "SHARPEST: the atmospheric turbulence profiling experiment using Shack–Hartmann sensor at the Subaru telescope," *Monthly Notices of the Royal Astronomical Society* **527**(2), 1831–1846 (2024).

[23] Laidlaw, D. J., Reeves, A. P., Singhal, H., and Calvo, R. M., "Characterizing turbulence profile layers through celestial single-source observations," *Applied Optics* **61**(2), 498–504 (2022).

[24] Caccia, J. L., Azouit, M., and Vernin, J., "Wind and CN2 profiling by single-star scintillation analysis," *Applied Optics* **26**, 1288 (Apr. 1987).

[25] Copernicus Climate Change Service, Climate Data Store, "ERA5 hourly data on pressure levels from 1940 to present," (2023). Copernicus Climate Change Service (C3S) Climate Data Store (CDS), DOI: 10.24381/cds.bd0915c6.

[26] Quatresooz, F., Griffiths, R., Bardou, L., Wilson, R., Osborn, J., Vanhoenacker-Janvier, D., and Oestges, C., "Continuous daytime and nighttime forecast of atmospheric optical turbulence from numerical weather prediction models," *Optics Express* **31**(21), 33850–33872 (2023).